J. Phys. D: Appl. Phys. 28 (1995) 2522–2528. Printed in the UK

# A dynamical diffraction approach to grazing-incidence x-ray diffraction by multilayers with lateral lattice misfits

**A P Ulyanenkov†‡, S A Stepanov†§, U Pietsch‡ and R Köhler§**

† Institute for Nuclear Problems, Bobruiskaya 11, Minsk SU-220050, Belarus
‡ Institut für Festkörperphysik der Universität Potsdam, Am Neuen Palais 10, Potsdam D-14415, Germany
§ MPG-AG 'Röntgenbeugung', Hausvogteiplatz 5-7, D-10117 Berlin, Germany

Received 23 June 1995, in final form 28 September 1995

**Abstract.** A method is presented for the computation of x-ray grazing-incidence diffraction in multilayers with lateral lattice mismatch. This method is based on the dynamical diffraction theory and on a matrix form of boundary conditions. Numerical examples are given to prove the validity of the theory. In present form the algorithm can be used for computing grazing-incidence diffraction by completely relaxed superlattices. The possibilities of extending this method to partially relaxed multilayers are discussed.

## 1. Introduction

In recent years, interest in studies of semiconductor superlattices (SL) and multilayers (ML) has grown. X-ray diffraction has proved to be a powerful technique for these studies since it can provide direct data on structural perfection, relaxation phenomena, and various defects in MLs (see, [1,2] and references therein). However, conventional x-ray diffraction methods sometimes fail for thin MLs because of known drawbacks: (i) the structural information is averaged over a depth of about 1 $\mu$m, which often exceeds the thickness of the ML; (ii) the signal from thin MLs is very small compared with the signal from the substrate due to the great penetration depth of x-rays; (iii) the measurements basically give the variations of lattice spacing perpendicular to the surface, whereas the stress relaxations in MLs take place in the lateral direction.

All these drawbacks have recently been overcome with the development of grazing-incidence x-ray diffraction (GID). GID provides information on surface layers as thin as 1–100 nm; the information is depth-selective depending on the incidence angle and the lateral strains are measured directly [3,4]. Using GID, one can also study the degree of crystalline disorder (amorphization) and interfacial roughness [5,6].

Unfortunately, there have not been so many applications of GID [3,7–15]. Two factors impede these applications: the high losses of intensity because of double-plane x-ray collimation and grazing incidence and the lack of general theoretical models for quantitative data analysis. Due to the former factor, the experiments basically require synchrotron radiation and the resolution of measurements has been relatively low. The majority of experiments has been concerned with unrelaxed GaAs/AlAs superlattices and other structures exhibiting no lattice misfits [9–11, 13, 14]. Only a few experiments [3,7,8] have studied the effect of stress relaxation and the resolution with respect to $\Delta a/a$ was no better than about 1%. The theoretical problems with GID have been due to the fact that the Takagi–Taupin equations [16, 17] commonly used for data analysis in x-ray diffraction are not applicable to GID. The wavefield amplitudes in GID vary with depth at length scales of about 1–10 nm (by a factor of $10^3$ shorter than in usual x-ray diffraction) and one cannot neglect the second-order derivatives of these amplitudes, as in the Takagi–Taupin approach. This problem has recently been overcome by the development of a matrix approach to GID [6, 13, 14, 18].

There is a significant difference in the effects of normal (vertical) and lateral lattice mismatch in MLs. The vertical lattice mismatch over a wide range does not cause structure defects, whereas the appearance of a lateral lattice mismatch is generally related to misfit dislocations or to the formation of 3D domains [7, 8, 15]. Here, SIMOX (silicon-on-insulator formed by oxygen ion implantation) structures [19, 20] are an exception due to the presence of an amorphous buffer between the layers with different lateral lattice spacing [21]. However, lateral strains always cause a discontinuity of the Bragg planes. The matrix dynamical diffraction theory of GID by MLs with vertical variation of lattice spacing was given in [18], whereas in the case of lateral strains only a few works are available for very simple bicrystal structures [22–25]. The complexity of the problem was sometimes the origin of false suggestions that the exit angle $\Phi_h$ of the diffracted waves in GID could directly give the lattice mismatch [25].

0022-3727/95/122522+07$19.50 

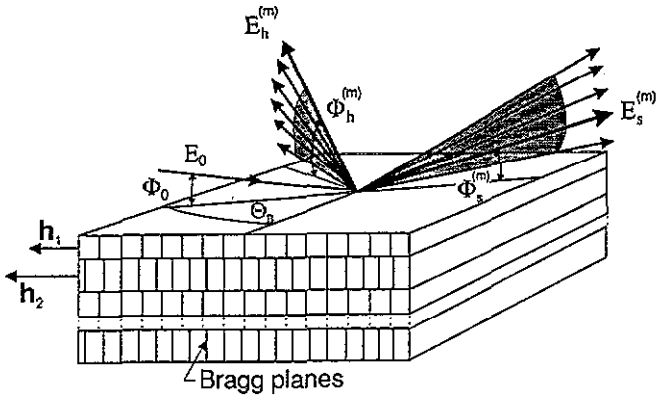


**Figure 1.** A schematic view of GID in the case of a superlattice consisting of two different components with mismatched lattice parameters.

In this paper we extend the matrix theory of GID to cases of lateral changes in crystal lattice spacing. As a simplest case we consider a ML to consist of two types of layers with different but constant lattice parameters. Our model is applicable to several kinds of structures: (i) samples like SIMOX ones [19, 20] in which the difference in the lattice spacings is accommodated without developing misfit dislocations or 3D domains [21], or (ii) completely relaxed two-component ML or SL systems with relatively thick layers in which the contribution of scattering at strain fields of misfit dislocations located near the interfaces can be neglected, compared to the scattering at the other parts of the layers. Our approach is based on the dynamical diffraction theory which is strongly suggested by the permanently increasing quality of MLs. The theoretical model is illustrated by several numerical examples. The limitations and possible extensions of the theory are also discussed when these examples are analysed.

## 2. Theory

In the case of large enough lateral mismatches the calculation of diffraction curves does not pose any serious problems because the diffraction processes on mismatched structures are separated [22]. The situation changes dramatically as soon as the splitting of GID Bragg peaks due to lateral lattice mismatch $\Delta a_\parallel/a$ becomes comparable with the halfwidth of these peaks. In this case the incident wave is very close to the Bragg condition for every layer and one cannot solve the dynamical diffraction problem separately for each layer because of the interference effects that have to be taken into account. First attempts to solve this problem for bicrystals were undertaken in [23]; the authors, however, did not succeed in the numerical implementation of their scheme.

Let us consider GID in a multilayered structure that consists of $N$ layers with two different lattice spacings: some of the layers are characterized by the reciprocal lattice vector $\boldsymbol{h}_1$ and the others have the vector $\boldsymbol{h}_2$ (figure 1). For simplicity, we suggest $h_{1z} = h_{2z}$ and $h_{1\parallel} \neq h_{2\parallel}$.

If the dynamical diffraction approach is applied, the incident and diffracted x-ray waves in each layer are connected with the dynamical diffraction equations at vectors $\boldsymbol{h}_1$ or $\boldsymbol{h}_2$. The boundary conditions at interfaces in multilayers require the preservation of lateral components of x-ray wavevectors in different layers. This requirement can only be met by expanding the wavefields into an infinite series of plane waves with respect to the difference $\Delta\boldsymbol{h} = \boldsymbol{h}_1 - \boldsymbol{h}_2$. Then the wavefields in vacuum, in $\boldsymbol{h}_1$ and in $\boldsymbol{h}_2$ layers can be written as

$$
\begin{aligned}
E^v(\boldsymbol{r}) &= E_0 \exp(\mathrm{i}\kappa_0\Phi_0 z)\exp(\mathrm{i}\kappa_{0\parallel}\rho) \\
&\quad + \sum_{m=-\infty}^{\infty}\{E_s^{(m)}\exp(-\mathrm{i}\kappa_0\Phi_s^{(m)}z)\exp[\mathrm{i}(\kappa_0 + m\Delta h)\rho] \\
&\quad + E_h^{(m)}\exp(-\mathrm{i}\kappa_0\Phi_h^{(m)}z)\exp[\mathrm{i}(\kappa_0 + h_1 + m\Delta h)\rho]\} \\
D^{h_1}(\boldsymbol{r}) &= \sum_{m=-\infty}^{\infty}\sum_{j=1}^{4}\{D_{0j,m}^{h_1}\exp(\mathrm{i}\kappa_0 u_{jm}^{h_1} z) \\
&\quad \times \exp[\mathrm{i}(k_{01} + m\Delta h)\rho] + D_{hj,m}^{h_1}\exp[\mathrm{i}\kappa_0(u_{jm}^{h_1} + \psi^{h_1})z] \\
&\quad \times \exp[\mathrm{i}(k_{01} + h_1 + m\Delta h)\rho]\} \\
D^{h_2}(\boldsymbol{r}) &= \sum_{m=-\infty}^{\infty}\sum_{j=1}^{4}\{D_{0j,m}^{h_2}\exp(\mathrm{i}\kappa_0 u_{jm}^{h_2} z) \\
&\quad \times \exp[\mathrm{i}(k_{02} + m\Delta h)\rho] + D_{hj,m}^{h_2}\exp[\mathrm{i}\kappa_0(u_{jm}^{h_2} + \psi^{h_2})z] \\
&\quad \times \exp[\mathrm{i}(k_{02} + h_2 + m\Delta h)\rho]\}. \qquad (1)
\end{aligned}
$$

In the following, a set of waves with index $m$ is called a harmonic of $m$th-order. In equation (1), the parameters $D_{0j,m}^{h_k}$ and $D_{hj,m}^{h_k}$ are the transmitted and the diffracted wave amplitudes in the $h_k$-type layer; they are related to the dynamical diffraction equations:

$$
D_{hj,m}^{h_k} = \frac{u_{jm}^{h_k\,2} - \Phi_s^{(m)} - \chi_0^{h_k}}{\chi_h^{h_k}} D_{0j,m}^{h_k} \equiv \upsilon_{j,m}^{h_k} D_{0j,m}^{h_k}. \qquad (2)
$$

Here $u_{jm}^{h_k}$ are the solutions to the dispersion equation:

$$
(u_{jm}^{h_k\,2} - \Phi_s^{(m)2} - \chi_0^{h_k})[(u_{jm}^{h_k} + \psi^{h_k})^2 - \Phi_h^{(m)2} - \chi_0^{h_k}] = \chi_h^{h_k}\chi_{\bar{h}}^{h_k} \qquad (3)
$$

where the parameters $\chi_0^{h_k}$, $\chi_h^{h_k}$ and $\chi_{\bar{h}}^{h_k}$ are the Fourier components of x-ray dielectric susceptibility, $\psi^{h_k}$ are the angles between $\boldsymbol{h}_k$ and the surface (see [14] for more details), $\boldsymbol{r} = (\rho, z)$, $\rho$ is the in-plane coordinate vector and $z$ is the coordinate along the internal surface normal; $\kappa_0$ and $\kappa_{0\parallel}$ are the incident wavevector and its lateral component in vacuum, respectively; $E_{s,h}^{(m)}$ are the amplitudes of the waves of the $m$th harmonic in vacuum; $\Phi_0$ is the incidence angle and $\Phi_{s,h}^{(m)}$ are the exit angles for the specularly reflected ($s$) and the diffracted ($h$) $m$-waves in vacuum. For these angles the following equations can be found [23] due to the preservation of lateral components of the wavevectors at interfaces:

$$
\begin{aligned}
\Phi_h^{(m)2} &= (\Phi_0 + \psi^{h_1})^2 - \alpha_{h_1} - m\Delta\alpha_h \\
\Phi_s^{(m)2} &= \Phi_0^2 - m\Delta\alpha_s \\
\Delta\alpha_s &= [(\kappa_0 + \Delta h_\parallel)^2 - \kappa_0^2]/\kappa_0^2 \\
\Delta\alpha_h &= \Delta\alpha_s + 2h_1\Delta h_\parallel/\kappa_0^2 \qquad (4)
\end{aligned}
$$

and $\alpha_{h_1} = [(k_{01}+h_1)^2 - k_{01}^2]/k_{01}^2$ is the parameter describing the deviation of the incident wave from the exact Bragg condition for the $h_1$-type layer.

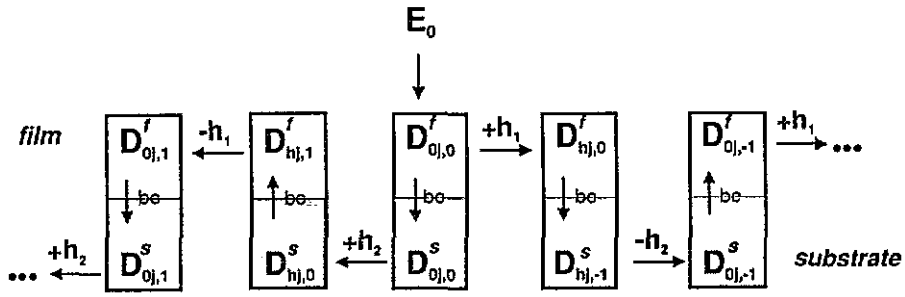


**Figure 2.** The multiwave reflection process in a bicrystal. 'bc' means boundary conditions and the transitions '$\pm h_1$' and '$\pm h_2$' denote the relations by means of the dynamical diffraction equations.

As follows from equation (4), instead of a single diffracted wave and a single reflected wave, our model gives two fans of the waves $E_s^{(m)}$ and $E_h^{(m)}$, with every wave leaving the crystal with its own exit angle $\Phi_s^{(m)}$ and $\Phi_h^{(m)}$, respectively. These vacuum waves by way of boundary conditions are connected with the set of waves $D_{jm}^{h_1,h_2}$ inside the ML.

From the physical point of view, the above model can be interpreted as the appearance of multiwave reflections which have their origin in the incident wave $E_0$. The harmonics formation process is illustrated in figure 2 for the simplest case of structure consisting of two layers only with reciprocal-lattice vectors $\boldsymbol{h}_1$ and $\boldsymbol{h}_2$. Here 'bc' means boundary conditions for given amplitudes; '$\pm h_1$' and '$\pm h_2$' mean the relations between amplitudes through the dynamical diffraction equations (2). The process develops as follows. The incident wave $E_0$ excites the transmitted waves $D_{0j,0}^f$ and $D_{0j,0}^s$ in the film and in the substrate, respectively. These waves give rise to the diffracted waves $D_{hj,0}^f$ and $D_{hj,0}^s$ with the wavevectors $\boldsymbol{\kappa}_0 + \boldsymbol{h}_1$ in the film and $\boldsymbol{\kappa}_0 + \boldsymbol{h}_2$ in the substrate. The waves $D_{hj,0}^f$ penetrating in turn into the substrate experience the Bragg diffraction at vector $-\boldsymbol{h}_2$ and give rise to the waves $D_{0j,-1}^s$ of the $-1$th harmonic with the wavevectors $\boldsymbol{\kappa}_0 + \boldsymbol{h}_1 - \boldsymbol{h}_2 = \boldsymbol{\kappa}_0 - \Delta\boldsymbol{h}$ directed along the direction of propagation of the transmitted and specularly reflected waves. Furthermore, these waves generate the waves $D_{hj,-1}^s$ with the wavevectors $\boldsymbol{\kappa}_0 + \boldsymbol{h}_1 - \Delta\boldsymbol{h}$ due to the dynamical diffraction process in the substrate, and so on. The same process occurs in the left branch of figure 2. Obviously, the multiple scattering is possible only in the case of strong Bragg diffraction of all harmonics and takes place in close proximity to the Bragg peaks, which requires the application of the dynamical diffraction theory.

Assuming that all the layers are crystalline, the boundary conditions for the wavefields and their derivatives at the bounds vacuum–$h_1$-type layer, $h_1$-type layer–$h_2$-type layer and $h_2$-type layer–$h_1$-type layer can be written as follows:

$$\delta_{m0}E_0 + E_s^{(m)} = \sum_{j=1}^{4} D_{jm}^{h_1}$$

$$E_h^{(m)} = \sum_{j=1}^{4} D_{jm}^{h_1} v_{jm}^{h_1}$$

$$\delta_{m0}\Phi_0 E_0 - \Phi_s^{(m)} E_s^{(m)} = \sum_{j=1}^{4} D_{jm}^{h_1} u_{jm}^{h_1}$$

$$-\Phi_h^{(m)} E_h^{(m)} = \sum_{j=1}^{4} D_{jm}^{h_1} \omega_{jm}^{h_1}$$

$$\sum_{j=1}^{4} D_{jm}^{h_1} \exp(\mathrm{i}\kappa_0 u_{jm}^{h_1} z_k) = \sum_{j=1}^{P} D_{jm}^{h_2} \exp(\mathrm{i}\kappa_0 u_{jm}^{h_2} z_k)$$

$$\sum_{j=1}^{4} D_{jm}^{h_1} v_{jm}^{h_1} \exp(\mathrm{i}\kappa_0 u_{jm}^{h_1} z_k) = \sum_{j=1}^{P} D_{jm-1}^{h_2} v_{jm-1}^{h_2} \exp(\mathrm{i}\kappa_0 u_{jm-1}^{h_2} z_k)$$

$$\sum_{j=1}^{4} D_{jm}^{h_1} u_{jm}^{h_1} \exp(\mathrm{i}\kappa_0 u_{jm}^{h_1} z_k) = \sum_{j=1}^{P} D_{jm}^{h_2} u_{jm}^{h_2} \exp(\mathrm{i}\kappa_0 u_{jm}^{h_2} z_k)$$

$$\sum_{j=1}^{4} D_{jm}^{h_1} \omega_{jm}^{h_1} \exp(\mathrm{i}\kappa_0 u_{jm}^{h_1} z_k) = \sum_{j=1}^{P} D_{jm-1}^{h_2} \omega_{jm-1}^{h_2} \exp(\mathrm{i}\kappa_0 u_{jm-1}^{h_2} z_k)$$

$$\sum_{j=1}^{4} D_{jm}^{h_2} \exp(\mathrm{i}\kappa_0 u_{jm}^{h_2} z_k) = \sum_{j=1}^{P} D_{jm}^{h_1} \exp(\mathrm{i}\kappa_0 u_{jm}^{h_1} z_k)$$

$$\sum_{j=1}^{4} D_{jm-1}^{h_2} v_{jm-1}^{h_2} \exp(\mathrm{i}\kappa_0 u_{jm-1}^{h_2} z_k) = \sum_{j=1}^{P} D_{jm}^{h_1} v_{jm}^{h_1} \exp(\mathrm{i}\kappa_0 u_{jm}^{h_1} z_k)$$

$$\sum_{j=1}^{4} D_{jm}^{h_2} u_{jm}^{h_2} \exp(\mathrm{i}\kappa_0 u_{jm}^{h_2} z_k) = \sum_{j=1}^{P} D_{jm}^{h_1} u_{jm}^{h_1} \exp(\mathrm{i}\kappa_0 u_{jm}^{h_1} z_k)$$

$$\sum_{j=1}^{4} D_{jm-1}^{h_2} \omega_{jm-1}^{h_2} \exp(\mathrm{i}\kappa_0 u_{jm-1}^{h_2} z_k) = \sum_{j=1}^{P} D_{jm}^{h_1} \omega_{jm}^{h_1} \exp(\mathrm{i}\kappa_0 u_{jm}^{h_1} z_k) \qquad (5)$$

where $\omega_{jm}^{h_k} \equiv v_{jm}^{h_k}(u_{jm}^{h_k} + \psi^{h_k})$ and $z_k$ are interface coordinates; $D_{jm}^{h_k} \equiv D_{0jm}^{h_k}$ and $D_{hjm}^{h_k}$ are expressed through $D_{0jm}^{h_k}$ by (2); $\delta_{m0}$ is the Kronecker symbol; $P = 2$ for the last layer in the SL (substrate), and $P = 4$ for the other layers (see the thick-crystal approximation in [14]).

The boundary conditions (5) give rise to mixing of the neighbouring harmonics on the bounds of layers with

different lateral components of the reciprocal-lattice vector. This is the reason why we cannot find the field amplitudes $E_s^{(m)}$ and $E_h^{(m)}$ separately for every harmonic $m$ and have to solve simultaneously the infinite system of related equations for an infinite number of harmonics. However, proceeding from general physical considerations, it is clear that the intensity loss process occurs with every reflection (figure 2). This fact enables us to neglect the higher order harmonics because of their low contribution to the intensity and we can cut off the harmonics spreading process.

For the practical implementation of this algorithm one has to find the central harmonic in terms of a maximum contribution to intensity and to determine how many harmonics should be taken into account in the positive and negative directions from the central one. The answer to the first question is simple: either zeroth- or first-order-harmonics are always central, representing the direct diffraction on $h_1$- or $h_2$-type layers, respectively.

The choice of the number of harmonics taken into account in both directions proceeds from the following condition:

$$\alpha^{\pm} = |\alpha_{h_1} \pm m^{\pm}\Delta\alpha_h| \gg 1 \tag{6}$$

where $m^{\pm}$ are the number of negative and positive harmonics. The condition of a large deviation from the Bragg condition ($\alpha^{\pm} \gg 1$) is adequately satisfied in practice when $\alpha^{\pm} > 5$.

Using the above approximations, the boundary conditions (5) for the finite number of harmonics $M = m^+ + m^-$ can be rewritten in a more convenient matrix form [14]:

$$\begin{aligned} S^v E^v &= S^1_{(U)} D^1 \\ S^1_{(L)} D^1 &= S^2_{(U)} D^2 \\ S^2_{(L)} D^2 &= S^3_{(U)} D^3 \\ &\cdots\cdots \\ S^{N-1}_{(L)} D^{N-1} &= S^N_{(U)} D^N. \end{aligned} \tag{7}$$

Matrices $S^k_{(U,L)}$ on the upper ($U$) and lower ($L$) bounds for the $h_1$-type layer are presented in a block-structure:

$$\begin{pmatrix} \boxed{-m^-} & & & \\ & \boxed{-m^- + 1} & & \\ & \cdots & & \\ & & \boxed{m^+ - 1} & \\ & & & \boxed{m^+} \end{pmatrix} \tag{8}$$

where the indices in the blocks mean that the block elements belong to the $m$th harmonic. Every $m$th block consists of the following matrix (we drop the indices $h_1$ and $(U, L)$ in the matrix elements):

$$\begin{pmatrix} e_1^{(m)} & e_2^{(m)} & e_3^{(m)} & e_4^{(m)} \\ V_1^{(m)} & V_2^{(m)} & V_3^{(m)} & V_4^{(m)} \\ U_1^{(m)} & U_2^{(m)} & U_3^{(m)} & U_4^{(m)} \\ W_1^{(m)} & W_2^{(m)} & W_3^{(m)} & W_4^{(m)} \end{pmatrix}. \tag{9}$$

The matrix block-structure for the $h_2$-type layer is quite different due to the mixing of harmonics:

$$\begin{pmatrix} \boxed{-m^- - 1, -m^-} & & & \\ & \boxed{-m^-, -m^- + 1} & & \\ & & \cdots & \\ & & \boxed{m^+ - 2, m^+ - 1} & \\ & & & \boxed{m^+ - 1, m^+} \end{pmatrix} \tag{10}$$

and the rectangular blocks are

$$\begin{pmatrix} 0 & 0 & 0 & 0 & e_1^{(m)} & e_2^{(m)} & e_3^{(m)} & e_4^{(m)} \\ V_1^{(m-1)} & V_2^{(m-1)} & V_3^{(m-1)} & V_4^{(m-1)} & 0 & 0 & 0 & 0 \\ 0 & 0 & 0 & 0 & U_1^{(m)} & U_2^{(m)} & U_3^{(m)} & U_4^{(m)} \\ W_1^{(m-1)} & W_2^{(m-1)} & W_3^{(m-1)} & W_4^{(m-1)} & 0 & 0 & 0 & 0 \end{pmatrix}. \tag{11}$$

Here the following notations are used:

$$\begin{aligned} e_j^{(m)} &= \exp(\mathrm{i}u_{jm}\kappa_0 z_{(U,L)}) \qquad U_j^{(m)} = u_{jm} e_j^{(m)} \\ V_j^{(m)} &= v_{jm} e_j^{(m)} \qquad W_j^{(m)} = \omega_{jm} e_j^{(m)}. \end{aligned} \tag{12}$$

The values $v_{jm}$, $u_{jm}$ and $\psi$ in the matrices (9) and (11) are correspondingly evaluated for $h_1$-type and $h_2$-type layers. $D^k$ is the vector of $4M$ size for the $h_1$-type layer and of $4M + 4$ size for the $h_2$-type layer:

$$\begin{aligned} D^k = (\ldots, &D^k_{01,m-1}, D^k_{02,m-1}, D^k_{03,m-1}, D^k_{04,m-1}, D^k_{01,m}, \\ &D^k_{02,m}, D^k_{03,m}, D^k_{04,m}, \ldots). \end{aligned} \tag{13}$$

The left-hand side in the first equation in (7) can be represented as follows:

$$S^v E^v = S^{vm} E^{vm} + E^0$$

where the matrix $S^{vm}$ is a block-constructed one of size $(4M \times 2M)$:

$$\begin{pmatrix} \boxed{-m^-} & \\ \cdots & \\ & \boxed{m^+} \end{pmatrix} \tag{14}$$

and the $m$th block is represented as

$$\begin{pmatrix} 1 & 0 \\ 0 & 1 \\ -\Phi_s^{(m)} & 0 \\ 0 & -\Phi_h^{(m)} \end{pmatrix}. \tag{15}$$

The vectors $E^{vm}$ and $E^0$ are

$$E^{vm} = (\ldots, E_s^{(m-1)}, E_h^{(m-1)}, E_s^{(m)}, E_h^{(m)}, \ldots)$$

$$E^0 = (\ldots, [E_0 = 1, 0, \Phi_0 E_0, 0], \ldots). \qquad (16)$$

The block [...] in (16) is placed where the zeroth harmonic occurs.

It is evident from (5) that the matrices $S^k_{(U,L)}$ for $h_1$-type layers have the dimension $(4M \times 4M)$ and the number of fields under consideration is equal to $4M$. For $h_2$-type layers we have $4M + 4$ fields (due to mixing of harmonics) and consequently the size of the matrices $S^k_{(U,L)}$ for layers of this type is $(4M \times 4M + 4)$. For a successful use of the matrix approach, it is necessary to match the number of variables with the number of equations. For this purpose, we use the amorphous layer approximation for the boundary harmonics. We cut off the process of harmonics multiplication in the $h_2$-type layer, so that only the two last transmitted fields $D^{h_2}_{0j,m^+}$ for the positive boundary harmonic and the two last diffracted fields $D^{h_2}_{hj,-m^-}$ for the negative boundary harmonic remain. This means that all the higher order waves do not undergo the diffraction process in the crystalline structure and, instead, propagate as waves in an amorphous layer. Thus, using the above procedure we have obtained a set of boundary conditions at every interface consisting of $4M$ equations.

Now, using the procedure developed in [14] and taking into account the fact that the substrate matrix is of size $(4M \times 2M)$ due to the dynamical thick-crystal approximation, [14] we obtain

$$T D^N - S^{vm} E^{vm} = E^0 \qquad (17)$$

with

$$T = S^1_{(U)}(S^1_{(L)})^{-1} S^2_{(U)}(S^2_{(L)})^{-1} \ldots S^N_{(U)}. \qquad (18)$$

Equation (17) is the system of $4M$ equations for $4M$ variables $E_s^{(m)}$, $E_h^{(m)}$, $D^N_{01,m}$ and $D^N_{02,m}$; $m = [-m^- \ldots m^+]$. The solution to this system provides us with a set of field amplitudes $E_h^{(m)}$ and $E_s^{(m)}$ in vacuum for the diffracted and the specularly reflected wave fans. The equations relating the intensities to the field amplitudes and the exit angles $\Phi_h^{(m)}$ are well known [18].

Let us consider now the limiting cases of our model at $\Delta a_\parallel/a \to \infty$ and $\Delta a_\parallel/a \to 0$. In the first case, the algorithm is reduced to the two-beam case of separate diffractions on layers with different lattice spacings. In the second case the application of our model is restricted because of the infinitely increasing number of harmonics which cannot be implemented numerically. This increase corresponds to a degeneration of the basis of our expansion in terms of $\exp(\Delta h r)$. The condition for the applicability of the model is

$$M|\Delta\alpha_h| \gg |\chi_h| \qquad (19)$$

where $M$ is the maximum number of harmonics taken in the computer program. The condition (19) means the width of our expansion exceeds the halfwidth of Bragg peaks. In the majority of cases (19) gives $\Delta a_\parallel/a \gtrsim 10^{-6}$.

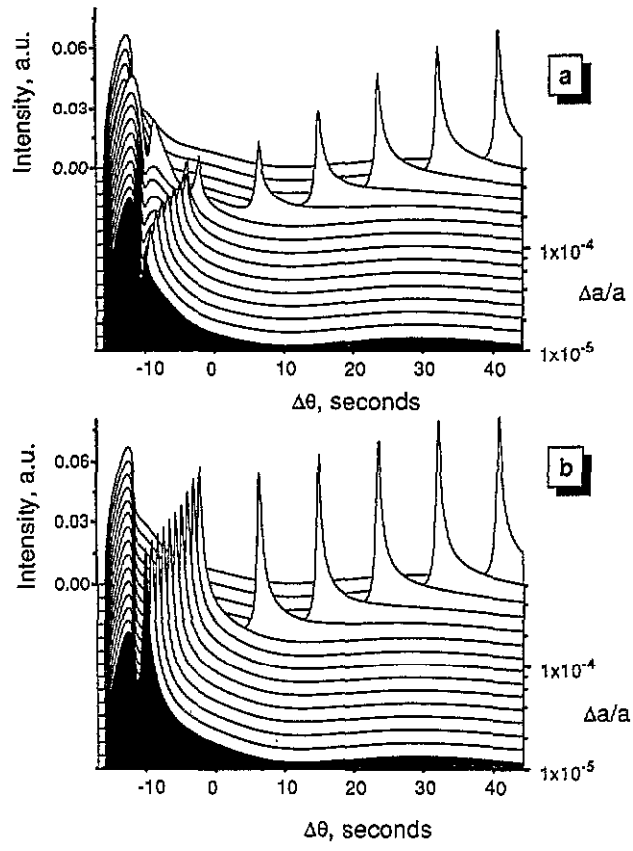


**Figure 3.** The variation of GID curves from a bicrystal in terms of their dependence on the mismatch parameter $\Delta a_\parallel/a$. The curves (a) are calculated in the framework of the model presented and the set of curves (b) is calculated assuming an independent diffraction process in every component of the bicrystal. The parameters of the calculations are given in the text.

## 3. Numerical examples and discussion

Diffraction curves for a bicrystal with two laterally mismatched lattice parameters were computed in two different ways. Figure 3 shows the set of diffraction curves for $\Theta$-scans in terms of their dependence on the parameter $\Delta a_\parallel/a$, thus describing the effect of lateral lattice strain on GID. The calculations were carried out for a structure consisting of a GaAs film (thickness 14.6 nm) being grown on GaAs [001] substrate. The lattice parameters of the film and the substrate were supposed to be mismatched by $\Delta a_\parallel$. The other input data were: (220) Bragg planes, $\sigma$-polarization, x-ray wavelength $\lambda = 0.154$ nm and the incidence angle $\Phi_0 = 0.6°$. Figure 3(b) demonstrates the diffraction curves calculated under the assumption of independent diffraction in both layers. In this case the dynamical diffraction problem is solved for every layer separately and not with respect to $\Delta a_\parallel/a$. Figure 3(a) represents the same diffraction curves calculated by the method described in section 2, namely with respect to interference effects during the Bragg diffraction in the bicrystal. As seen in figure 3, there are considerable differences in the diffracted beam intensities within the region of small $\Delta a_\parallel/a$, for which the Bragg condition is nearly satisfied for both layers. Figure 4 shows the section of figure 3 at $\Delta a_\parallel/a = 10^{-4}$. The ratio of the Bragg

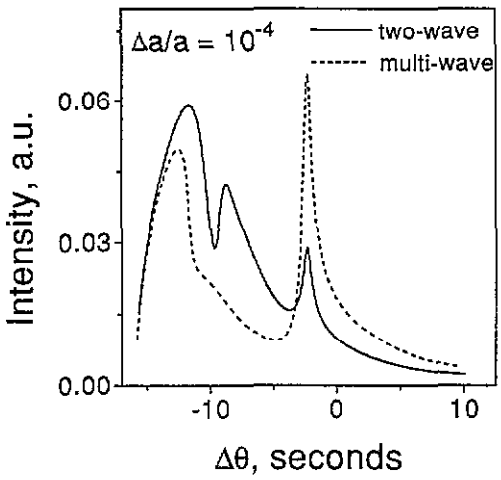


**Figure 4.** The sections from 3D curves of figure 3, representing the appearance of an additional peak at small $\Delta a_{\parallel}/a = 1 \times 10^{-4}$ in our model.

peak intensities in our model is opposite to that of the two-wave model, and an additional interference peak between the main Bragg peaks for film and substrate appears in our calculations.

Figure 5 demonstrates the $\Phi_h$ scans for a SL, consisting of 20 periods of thin GaAs and AlAs layers on a GaAs [001] substrate. The thickness of the layers in the SL is 14.6 nm of AlAs and 6.8 nm of GaAs. The calculations were carried out with the following input data: the beam incidence angle $\Phi_0 = 0.35°$, the Bragg planes were (220), the miscut angle of the surface with respect to the (001) plane was $\psi^h = -0.03°$ and the x-ray wavelength $\lambda = 0.154$ nm. This structure was analysed earlier in a number of papers [14, 26]. Curves 5(a) and (d) present the limiting cases of our model. First, one can compare the diffraction curve calculated by our program (circles) for a greatly mismatched AlAs lattice ($\Delta a_{\parallel}/a = 10^{-2}$) and the diffraction curve calculated for the SL, when assuming independent diffraction in both components of the SL. The latter assumption implies that, in turn, one of two kinds of layers is treated as being amorphous due to weak diffraction and then the intensities are added. No interference effects are displayed by our model. Figure 5(d) illustrates the limit of $\Delta a_{\parallel}/a = 0$, namely a completely unrelaxed structure. The curve is calculated according to [18] and our theory is not presented since it is degenerated according to equation (19). However, the curves in figures 5(b) and (c) calculated according to our theory for $\Delta a_{\parallel}/a = 10^{-3}$ and $10^{-4}$, respectively, exhibit the transformation of the shape with decreasing $\Delta a_{\parallel}/a$ from the case in figure 5(a) to that in figure 5(d). One can see that the shape of these $\Phi_h$ scans is clearly sensitive to the value of the lattice mismatch.

Thus, we can conclude that in the limiting case $\Delta a_{\parallel}/a \to \infty$ our model is reduced to the two-wave scattering scheme used in experimental data analysis of GID. The advantage of the proposed model is that it is possible to simulate structures with a lateral lattice misfit over a wide range of $\Delta a_{\parallel}/a$.

As follows from the given examples, the sensitivity of the GID method with respect to the lateral lattice mismatch

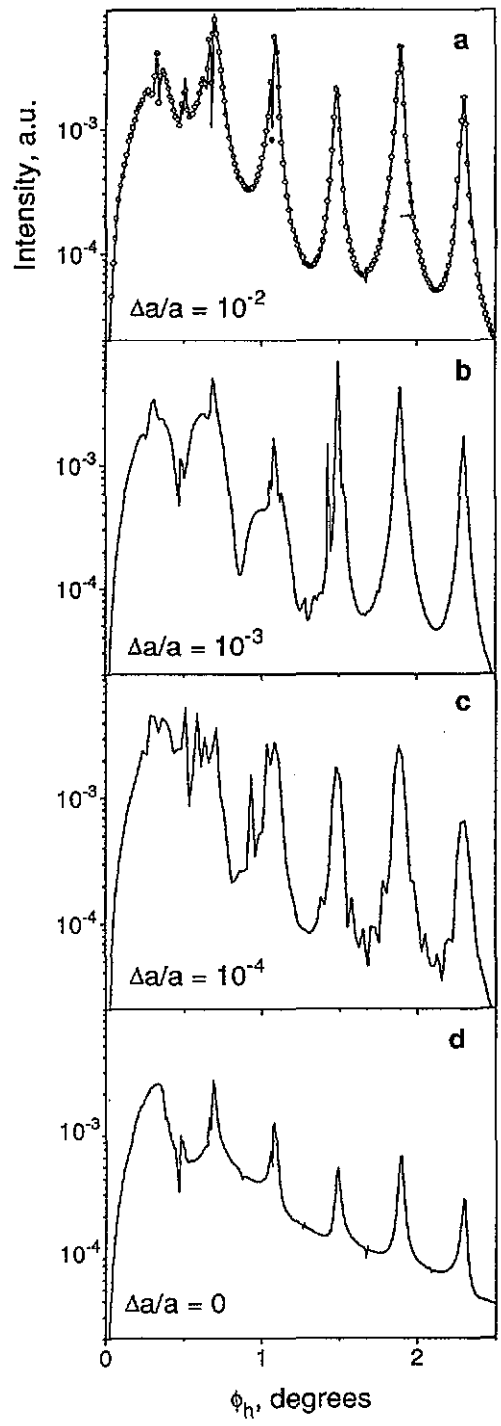


**Figure 5.** Theoretical calculations of $\Phi_h$ scans from a GaAs/AlAs superlattice for different $\Delta a_{\parallel}/a$: (a) $10^{-2}$, (b) $10^{-3}$, (c) $10^{-4}$ and (d) 0. In (a) our model is presented by circles and the full line corresponds to the two-wave approximation, which assumes independent diffraction in both superlattice components. In (d) our model is degenerated and the full line corresponds to two-beam diffraction by a completely matched structure.

is up to two orders of magnitude greater than that of conventional high-resolution x-ray diffractometry. This fact is due to the special shape of Bragg peaks in GID: they are different from the Darwin curve and can exhibit a very sharp maximum of halfwidth about $|\chi_{hi}|$ whereas the halfwidth of the whole peak is about $|\chi_{hr}|$, as usually.

The ratio $|\chi_{hi}/\chi_{hr}| \simeq 10^{-2}$ causes the variations in the fine structure of the Bragg peaks due to minor deviations in the lattice spacing and makes it possible to apply GID to investigations of the initial stages of relaxation in strained SLs and buried doped layer structures. However, up to now the application of the GID has been restricted to fully pseudomorphic heterostructures because of conceptional restrictions of computation models. These seem to have been overcome with the help of the method presented in this paper. We believe that our theoretical results will stimulate new applications of high-resolution GID experiments.

The theory given in the present form can be used for calculating GID from completely (uniformly) relaxed superlattices. However, our model can be easily extended from one $\Delta h = h_1 - h_2$ to the system that possesses a set of $\Delta h$: $\Delta h \rightarrow (\Delta h, 2\Delta h, 3\Delta h, \ldots)$. This extension provides the opportunity to model $\Delta h_\parallel$ profiles along the $z$ direction. The grazing-incidence diffraction from partially relaxed structures can be simulated with such an advanced model. The interface roughness effects can also be easily added to our model by analogy with [6]. Finally, the wavefields obtained by the developed scheme can be applied to calculating the x-ray scattering at strain fields produced by misfit dislocations near interfaces. In the case of a distance between dislocations much less than the thickness of layers, $a^2/\Delta a \ll t$, these strain fields can be treated as a perturbation to our model and the distorted wave Born approximation (DWBA) method [26–29] can be used. For $\Delta a/a \simeq 10^{-1}$ this estimation gives $t \gg 5$ nm.

## Acknowledgment

One of us (AU) thanks the Deutsche Forschungsgemeinschaft for support.

## References

[1] Fewster P F 1993 *Semicond. Sci. Technol.* **8** 1915
[2] Tanner B K and Bowen D K 1993 *J. Cryst. Growth* **126** 1
[3] Marra W C, Eisenberger P and Cho A Y 1979 *J. Appl. Phys.* **50** 6927
[4] Afanas'ev A M and Melkonyan M K 1983 *Acta Crystallogr.* A **39** 207
[5] Aleksandrov P A, Afanas'ev A M, Melkonyan M K and Stepanov S A 1984 *Phys. Status Solidi* a **81** 47
[6] Stepanov S and Köhler R 1994 *J. Appl. Phys.* **76** 7809
[7] Williams A A, Thornton J M C, Macdonald J E, van Silfhout R G, van der Veen J F, Finney M S, Johnson A D and Norris C 1991 *Phys. Rev.* **43** 5001
[8] Etgens V H, Sauvage-Simkin M, Pinchaux R, Massies J, Jedrecy N, Waldhauer A, Tatarenko S and Jouneau P H 1993 *Phys. Rev.* **47** 10607
[9] Melikyan O G, Imamov R M and Novikov D V 1992 *Solid State Phys. (Russia)* **4** 1572
[10] Pietsch U, Seifert W, Fornell J-O, Rhan H, Metzger H, Rugel S and Peisl J 1992 *Appl. Surf. Sci.* **54** 502
[11] Pietsch U, Metzger H, Rugel S and Robinson I K 1993 *J. Appl. Phys.* **74** 2381
[12] Rose D, Pietsch U, Gottschalch V and Rhan H 1995 *J. Phys. D: Appl. Phys.* **28** A246
[13] Rugel S, Wallner G, Metzger H and Piesl J 1993 *J. Appl. Crystallogr.* **26** 34
[14] Stepanov S A, Pietsch U and Baumbach G T 1995 *Z. Phys.* B **96** 341
[15] Rose D and Pietsch U 1995 *Mater. Res. Soc. Proc.* at press
[16] Takagi S 1962 *Acta Crystallogr.* **15** 1311; 1969 *J. Phys. Soc. Japan* **26** 1239
[17] Taupin D 1964 *Bull. Soc. Fr. Minér. Cristallogr.* **87** 469; 1967 *Acta Crystallogr.* **23** 25
[18] Stepanov S and Köhler R 1994 *J. Phys. D: Appl. Phys.* **27** 1923
[19] Sturm J C, Chen C K, Pfeiffer L and Hemment P L F 1987 *Mater. Res. Soc. Proc.* **107**
[20] Jaussaud C, Margail J, Lamure J M and Bruel M 1994 *Radiation Effects and Defects in Solids* **127** 319
[21] Prieur E, Haertwig J, Garcia A, Ohler M, Baruchel J, Aspar B and Rolland G 1995 *J. Crystal Growth* at press
[22] Aleksandrov P A, Afanas'ev A M and Stepanov S A 1984 *Poverkhn., Fiz. Khim. Mekh. USSR* **8** 9 (English translation 1985 *Phys. Chem. Mech. Surf.* **3** 2222)
[23] Aleksandrov P A and Stepanov S A 1986 *Poverkhn., Fiz. Khim. Mekh. USSR* **6** 117 (English translation 1990 *Phys. Chem. Mech. Surf.* **5** 1524)
[24] Melikyan O G 1991 *Kristallografiya* **36** 549
[25] Sakata O and Hashizume H 1991 *Rep. Res. Lab. Eng. Mater., Tokyo Inst. Technol.* **16** 27
[26] Holy V and Baumbach T 1994 *Phys. Rev.* B **49** 10668
[27] Vineyard G H 1982 *Phys. Rev.* B **26** 4146
[28] Sinha S K, Sirota E B, Garoff S and Stanley H B 1988 *Phys. Rev.* B **38** 2297
[29] Baumbach G T, Tixier S, Pietsch U and Holý V 1995 *Phys. Rev.* B **51** 16848